

Budgeted Adversarial Attack against Graph-Based Anomaly Detection in Sensor Networks

Sanju Xaviar
 University of Alberta
 Edmonton, AB, Canada
 xaviar@ualberta.ca

Omid Ardakanian
 University of Alberta
 Edmonton, AB, Canada
 oardakan@ualberta.ca

ABSTRACT

Graph Neural Networks (GNNs) have emerged as powerful models for anomaly detection in sensor networks, particularly when analyzing multivariate time series. In this work, we introduce BETA, a novel grey-box evasion attack targeting such GNN-based detectors, where the attacker is constrained to perturb sensor readings from a limited set of nodes, excluding the target sensor, with the goal of either suppressing a true anomaly or triggering a false alarm at the target node. BETA identifies the sensors most influential to the target node's classification and injects carefully crafted adversarial perturbations into their features, all while maintaining stealth and respecting the attacker's budget. Experiments on three real-world sensor network datasets show that BETA reduces the detection accuracy of state-of-the-art GNN-based detectors by 30.62 to 39.16% on average, and significantly outperforms baseline attack strategies, while operating within realistic constraints.

CCS CONCEPTS

- Security and privacy → *Intrusion/anomaly detection and malware mitigation*;
- Networks → **Sensor networks**.

KEYWORDS

Graph Neural Networks, Adversarial Attack, Anomaly Detection, Multivariate Time Series

ACM Reference Format:

Sanju Xaviar and Omid Ardakanian. 2025. Budgeted Adversarial Attack against Graph-Based Anomaly Detection in Sensor Networks. In *The xxth International Conference on xxx, TBD, 2025, TBD*. ACM, New York, NY, USA, 12 pages. <https://doi.org/xxxx>

1 INTRODUCTION

Sensor networks are ubiquitous in critical infrastructure systems, from water treatment plants and power grids to air quality monitoring and smart transportation. These networks continuously generate large volumes of time series data, often multimodal in nature, comprising readings from different sensors, collected at various locations and at high frequencies. Timely anomaly detection in such data streams is essential for ensuring the reliability

Permission to make digital or hard copies of all or part of this work for personal or classroom use is granted without fee provided that copies are not made or distributed for profit or commercial advantage and that copies bear this notice and the full citation on the first page. Copyrights for components of this work owned by others than the author(s) must be honored. Abstracting with credit is permitted. To copy otherwise, or republish, to post on servers or to redistribute to lists, requires prior specific permission and/or a fee. Request permissions from permissions@acm.org.

TBD '25, TBD, 2025, location TBD

© 2025 Copyright held by the owner/author(s). Publication rights licensed to ACM.
 ACM ISBN xxxx...\$15.00
<https://doi.org/xxxx>

and safety of these systems, enabling prompt intervention in the event of faults, intrusions, or system failures. However, detecting anomalies in multimodal time series is inherently challenging due to complex spatial and temporal dependencies that arise among heterogeneous sensor nodes and the sparsity of anomalies [47]. Traditional statistical and univariate approaches [31] often fail to capture these intricate interdependencies, necessitating more sophisticated models.

Graph Neural Networks (GNNs) have emerged as a powerful tool for anomaly detection in sensor networks, thanks to their ability to model dependencies between the sensors [14, 19, 20, 25, 26, 33, 44]. The sensor network is represented as a graph, where nodes correspond to individual sensors and edges reflect interdependencies, often learned from the data rather than imposed a priori. This graph-based representation allows anomaly detection to be framed as a node classification problem, where each sensor's status (normal or anomalous) is inferred based on its own readings and those of its neighbors. Recent advances, such as graph attention networks (GATs), have further enhanced the interpretability of these models by highlighting influential nodes and features [39–42]. Despite these strengths, GNN-based models are prone to adversarial attacks adding perturbations to sensor data to manipulate detection outcomes. These attacks raise pressing concerns about the robustness of such models in critical applications [37].

A growing body of work has begun to explore adversarial vulnerabilities in graph-based machine learning models that perform different tasks [11, 13, 36, 49]. Notably, the Nettack algorithm targets node classification tasks by injecting minimal perturbations into the graph structure or node features [48]. However, these attacks often assume full access to the target node, are not designed for time series data, or do not explicitly consider real-world constraints such as the attacker's budget. In contrast, the domain of image classification has explored budgeted adversarial attacks, such as the sparse perturbation attack exemplified by the one-pixel attack [35], where only a minimal subset of input features is perturbed. In sensor networks, an attacker needs to compromise a subset of sensors to influence the detection outcome for a target sensor. In practice, hacking into each sensor incurs a cost, and sensors installed at hotspots may be safeguarded either physically or through security measures (e.g., access control). This sets up a more realistic budgeted evasion attack scenario, where the attacker is constrained to perturb only a fixed number of sensors' readings. Prior work in sensor networks has largely overlooked these constraints [9, 16, 30, 37]. Our work addresses this critical gap by formulating and evaluating a budget-aware adversarial attack that operates under practical constraints.

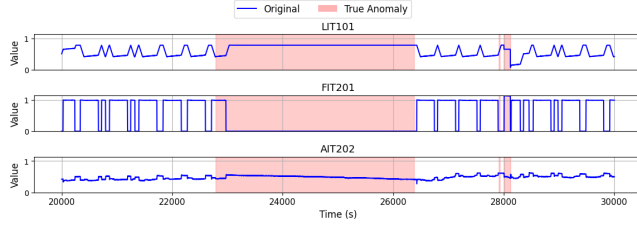


Figure 1: Visualization of readings of three sensors in the SWaT dataset, with anomalies highlighted in red.

In this paper, we propose Budgeted Explainability-guided Targeted Attack (BETA), a novel grey-box evasion attack against GNN-based anomaly detectors in sensor networks. BETA first employs GAFExplainer [45] on a surrogate anomaly detection model to find the subgraph most influential in determining the anomaly score of a target sensor, which is assumed to be safeguarded. If the subgraph size exceeds the attacker’s budget, a node selection heuristic based on eigenvector centrality is used to reduce the set of influencer nodes. We then use the Projected Gradient Descent (PGD) [28] algorithm to perturb only the features of the selected influencer nodes within the boundary of the infinity ball. We evaluate the effectiveness of our attack using two state-of-the-art GNN-based anomaly detection models—Graph Deviation Network (GDN) [14] and Topology-aware GDN (TopoGDN) [25]—on three real-world datasets from a six-stage industrial control system of a water treatment plant (SWaT); a water distribution testbed simulating cyber-physical attacks on industrial control systems (WADI); and a regional air quality monitoring network (SJVAir). Our contributions are summarized below:

- We introduce a budgeted, grey-box adversarial attack framework tailored to anomaly detection in sensor networks, reflecting realistic constraints on attacker capabilities.
- We combine GAFExplainer, a state-of-the-art GNN explainer that simultaneously considers graph topology and node features with a topology-aware heuristic (*i.e.* eigenvector centrality) to determine the best attack points for PGD given a surrogate model and a fixed attack budget, enabling effective and stealthy evasion attacks.
- We empirically validate our approach on three real-world multimodal sensor datasets, demonstrating its effectiveness against state-of-the-art GNN-based anomaly detection models under budget constraints. Compared to Netattack and a random attack, we show that BETA can significantly reduce the anomaly detection performance of representative GNN-based detectors.

Figure 1 shows the original readings of three representative sensors, *i.e.* LIT101 (tank level), FIT201 (flow) and AIT202 (chemical analyzer), from the SWaT dataset. The shaded regions indicate the true anomalous intervals as labeled in the dataset. Figure 2 illustrates how BETA adds imperceptible perturbations to readings of FIT201 and AIT202 so as to change the anomaly detection outcome for LIT101, which is assumed to be the target node. Despite adding no perturbations to readings of LIT101 directly, the GNN-based anomaly detector falsely detects anomalies and suppresses true anomalies that existed in the dataset.

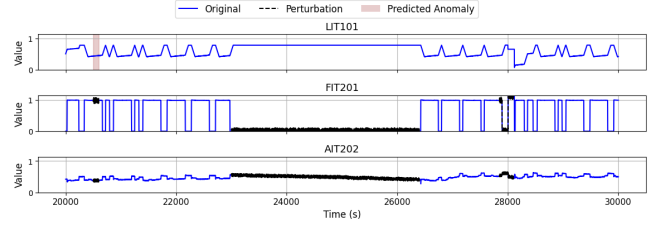


Figure 2: Visualization of perturbed sensor readings in the SWaT dataset. FIT201 and AIT202 are selected as influencer nodes for changing the anomaly detection result at LIT101.

2 RELATED WORK

2.1 Multivariate Time Series Anomaly Detection

Numerous approaches have been proposed for anomaly detection in multivariate time series [17]. They can be broadly classified into: (i) *reconstruction-based methods*, which detect anomalies based on the reconstruction error, *i.e.* the difference between the reconstructed data and the original sequence; (ii) *forecasting-based methods*, which rely on the deviation of the predicted value from the observed value; (iii) *self-supervised methods*, which learn from unlabeled data, often by contrasting positive and negative samples; and (iv) *hybrid methods*, which combine some of the above approaches.

Forecasting-based methods which are shown to consistently outperform reconstruction-based methods across a variety of anomaly detection benchmarks [14, 25]. Moreover, unlike self-supervised methods, they do not require a set of negative samples which may not truly represent the actual anomalies that exist in the dataset. Recent forecasting-based anomaly detection methods utilize a GNN [14, 22, 25], a transformer architecture [38], or both [12]. We consider two state-of-the-art forecasting-based methods, namely GDN [14] and TopoGDN [25], that utilize a GNN for capturing dependencies in multivariate time series. Specifically, they detect node-level anomalies in multivariate time series by leveraging graph representations and attention mechanisms to dynamically capture cross-sensor dependencies. It is worth noting that TopoGDN [25] outperforms transformer-based methods, such as TranAD [38], in the multivariate time series anomaly detection task.

2.2 Adversarial Attacks on Time Series Models

Adversarial attacks manipulate machine learning models by introducing carefully crafted perturbations to input data. The goal is to cause misclassification of data that belong to a specific class (targeted) or any class (untargeted). Adversarial attacks can also be classified based on the level of knowledge that the attacker has about the machine learning model into three categories: white-box, grey-box, and black-box attacks [11]. In a white-box attack, the attacker has full access to the model architecture and parameters, prediction results, and even gradient information during training. With this knowledge, the attacker can generate highly effective adversarial samples. In a grey-box attack, the attacker has only partial knowledge of the model, such as limited access to the model architecture or a subset of model parameters. In a black-box attack, the attacker has no information about the model; it has only query access to the model [36], *i.e.* it can observe the model’s output for

Table 1: Evasion attacks on multivariate time series anomaly detection models (D indicates a direct attack and I indicates an indirect attack through influencer nodes)

References	Attack	Attacker's Knowledge	D/I	Budgeted
Tariq et. al [37]	FGSM, PGD	White-box, Black-box	D	✗
Shaiik et. al [34]	FGSM, PGD, CW	White-box	D	✗
Goodge et. al [16]	FGSM	White-box	D	✗
Jia et. al [18]	FGSM	White-box	D	✗
Srinidhi et. al [27]	FGSM, BIM, PGD	White-box	D	✗
<i>BETA (Our approach)</i>	Constrained-PGD	Grey-box	I	✓

a given input. This query access is often used to train a surrogate model to perform the attack.

Adversarial attacks can be performed at training time (poisoning attacks) and at test time (evasion attacks). Evasion attacks, such as FGSM [15], BIM [21], PGD [28] and CW [10], mislead a trained model by modifying certain features in the input data. Graph-based evasion attacks, such as GradArgmax [13], may also alter links in the underlying graph based on gradient information from a surrogate model to deceive the classifier. Since it is easier to safeguard the training data and ensure that the graph structure used for classification remains intact, this work focuses on evasion attacks that add perturbations to sensor readings only. In particular, we propose a constrained PGD-based evasion attack tailored for anomaly detection, under the grey-box assumption, i.e. the attacker knows the graph structure of the GNN model used for anomaly detection.

2.2.1 Evasion Attacks on Graph Neural Networks. The most notable example of adversarial attacks against GNNs is Nettack [48], which focuses on misclassifying a specific set of target nodes. This attack is grey-box because it assumes access to the graph structure, node features, and the overall architecture of the target model, but not its parameters. The authors study poisoning or causative attacks, in addition to evasion attacks. Their approach involves generating adversarial perturbations that target both node features and the graph structure, accounting for dependencies between instances. In [46], an evasion attack, called projective ranking, is designed to generate transferable adversarial perturbations for graph neural networks. It incorporates mutual information to assess the long-term impact of perturbations. This approach enables transferable, structure-based (rather than feature-based) attacks across varying target nodes and perturbation budgets.

2.2.2 Evasion Attacks on Anomaly Detection Models. Table 1 summarizes the prior work on evasion attacks targeting multivariate time series anomaly detection models. Most previous work focuses on gradient-based attacks, such as FGSM and PGD, typically in a white-box setting where the model architecture and parameters are fully accessible. Moreover, all these attacks are direct, meaning that the features of the target node are directly perturbed, overlooking indirect manipulation and budgeted settings. In contrast, our approach proposes a constrained-PGD attack in a grey-box setting, capable of performing indirect perturbations under a strict budget, making it more practical and targeted for real-world multivariate anomaly detection scenarios. It is worth noting that PGD has been found to consistently outperform FGSM and other gradient-based evasion attacks in the multivariate case [27, 37], motivating us to build BETA on top of PGD.

3 PRELIMINARIES

We provide an overview of two state-of-the-art models for multivariate time-series anomaly detection that utilize graph structure learning and attention, namely the Graph Deviation Network (GDN) [14] and its extension, TopoGDN [25]. Specifically, GDN [14] detects anomalies by leveraging a GNN to capture both dependencies within the sensor data. It consists of two main components: a time series forecasting model and a threshold-based anomaly detection mechanism. The forecasting module uses GAT to predict future sensor readings based on historical data and learned relationships. The anomaly detection mechanism then evaluates discrepancies between predicted and actual readings, assigning anomaly scores accordingly. TopoGDN [25] extends GDN by incorporating a multi-scale temporal convolution module that captures fine-grained short and long-term temporal dependencies in sensor readings and a topological graph attention and pooling module that enhances structural representations by integrating higher-order topological features derived via persistent homology, while preserving the core architecture of GDN, described in Sections 3.1 to 3.3. The architectural enhancements specific to TopoGDN are detailed further in Sections 3.4 and 3.5.

3.1 Graph Structure Learning

Consider a multivariate time-series segment $\mathbf{X}^t = [\mathbf{x}_1^t, \dots, \mathbf{x}_N^t]^\top$, where N is the total of number of sensors and each \mathbf{x}_i^t collects historical data emitted by sensor i in a time window of length w , preceding time t :

$$\mathbf{x}_i^t = [x_i^{(t-w)}, \dots, x_i^{(t-1)}] \in \mathbb{R}^w \quad (1)$$

The model learns relationships among sensors using sensor embedding vectors $\mathbf{v}_i \in \mathbb{R}^d$ for each sensor i , which are initialized randomly and trained jointly with the rest of the model parameters via backpropagation. These embeddings define a similarity metric given by:

$$g_{ji} = \frac{\mathbf{v}_i^T \mathbf{v}_j}{\|\mathbf{v}_i\| \|\mathbf{v}_j\|} \mathbb{I}(j \in C_i) \quad (2)$$

where C_i represents a set of candidate connections for sensor i , $\|\cdot\|$ denotes the Euclidean norm, and the indicator function \mathbb{I} returns 1 when node j belongs to C_i and 0 otherwise. A graph adjacency matrix \mathbf{A} is then constructed by connecting each node to its M most similar neighbors, with respect to g_{ji} , where M defines the maximum number of edges a node can have, which is a hyperparameter.

3.2 GAT for Feature Extraction

The GDN model employs a GAT layer to dynamically aggregate information from a node's neighbors. For each node i , the aggregated representation \mathbf{r}_i^t is computed as:

$$\mathbf{r}_i^t = \text{ReLU} \left(\sum_{j: \mathbf{A}_{ji} > 0} \beta_{ij} \mathbf{W} \mathbf{x}_j^t \right) \quad (3)$$

where \mathbf{x}_j^t represents the feature vector of node j at time t , and $\mathbf{W} \in \mathbb{R}^{d \times w}$ is a learnable weight matrix. The attention coefficients β_{ij} are computed as:

$$\beta_{ij} = \frac{\exp(\rho_{ij})}{\sum_{k: \mathbf{A}_{ki} > 0} \exp(\rho_{ik})} \quad (4)$$

where

$$\rho_{ij} = \text{LeakyReLU} \left(\omega^\top \left((\mathbf{v}_i \oplus \mathbf{Wx}_i^t) \oplus (\mathbf{v}_j \oplus \mathbf{Wx}_j^t) \right) \right) \quad (5)$$

with a learnable parameter vector ω , and \oplus denoting concatenation.

3.3 Anomaly Detection Mechanism

Next, *anomaly scores* are computed based on forecasting errors. The prediction $\hat{x}^{(t)}$ is obtained by passing the aggregated node representations to a number of stacked fully-connected layers denoted as h_θ :

$$\hat{x}^{(t)} = h_\theta (\mathbf{v}_1 \odot \mathbf{r}_1^t, \dots, \mathbf{v}_N \odot \mathbf{r}_N^t), \quad (6)$$

where \odot denotes element-wise multiplication. For each sensor i , the prediction error is computed as:

$$\xi_{i,t} = \left| x_i^{(t)} - \hat{x}_i^{(t)} \right|, \quad (7)$$

and is standardized for consistency to obtain the anomaly score:

$$\tilde{\xi}_{i,t} = \frac{\xi_{i,t} - \text{Median}}{\text{IQR}}. \quad (8)$$

In the above equation, Median and IQR are respectively the median and interquartile range of $\xi_{i,t}$ across time. To compute the overall anomaly detection outcome at time step t , the prediction errors across sensors are aggregated using the max function, then compared against a threshold:

$$y^{(t)} = \mathbb{I} \left(\max_i (\tilde{\xi}_{i,t}) > \lambda \right), \quad (9)$$

where \mathbb{I} is an indicator function. Since we focus on *node-level* anomaly detection, we omit the hardmax aggregation in the last step to obtain the anomaly detection outcome for each node i at time t :

$$y_i^{(t)} = \mathbb{I} \left(\tilde{\xi}_{i,t} > \lambda \right).$$

3.4 Multi-Scale Temporal Convolution Module

TopoGDN captures multi-scale temporal patterns using 1D convolutions with varying receptive fields. It applies H different convolution filters, each with kernel size w_h ($1 \leq h \leq H$), to extract temporal features at different scales. The output of the h -th filter at time step t is computed as:

$$z_i^{(h)}[t] = \sum_{l=0}^{w_h-1} x_i^{(t+l)} \cdot f_h[l], \quad (10)$$

where $f_h[l]$ denotes the learnable weights of the h -th convolutional filter at position i . The aggregated output at time step t is then given by:

$$z_i[t] = \text{Pool} \left(z_i^{(1)}[t], z_i^{(2)}[t], \dots, z_i^{(H)}[t] \right), \quad (11)$$

where $\text{Pool}(\cdot)$ denotes a pooling operation (e.g., average or max), which merges the outputs of all convolution scales into a unified temporal representation for node i .

The resulting $\mathbf{z}_i^t = [z_i[t-w], \dots, z_i[t-1]] \in \mathbb{R}^w$ is then used instead of \mathbf{x}_i^t to compute the initial and aggregated node representations following Eq. 3.

3.5 Topological Graph Attention and Pooling Module

TopoGDN builds upon the standard GAT mechanism used in GDN (Section 3.2) by introducing two key enhancements. First, it integrates a learnable sensor embedding into the attention mechanism as an additional input and replaces the standard dot-product attention with a multi-layer perceptron (MLP). This design enables the model to capture complex and non-linear dependencies among sensors, which are often overlooked by simple attention mechanisms. Second, after computing attention-based node embeddings, TopoGDN applies a topological pooling module based on persistent homology. It extracts high-order topological features from a sequence of graph filtrations, embeds the resulting persistence diagrams into fixed-size vectors, and fuses them with the attention-based embeddings to enrich the structural representation. Each graph is viewed through R filtration functions, yielding a series of nested subgraphs $\mathcal{G}^{(r)} = \{G_r^{(0)} \subseteq \dots \subseteq G_r^{(L)}\}$. Nodes and edges are progressively filtered using thresholds $\theta_r^{(l)}$ and topological features are extracted via persistent homology. The resulting barcode diagrams $\mathcal{B}_r^{(d)}$, where $d \in \{0, 1\}$, are embedded into vector space using a transformation:

$$\Psi^{(d)} : \mathcal{B}_r^{(d)} \rightarrow \mathbb{R}^{N \times d}. \quad (12)$$

Here, N represents the number of sensor nodes and d represents the dimensionality of the embedding for each sensor node. This yields topological embeddings that are concatenated with attention-based features for downstream anomaly detection.

4 PROBLEM FORMULATION

We consider a sensor network that consists of N sensors installed at different locations, each generating real values at regular intervals. We model the dependency between these sensors using a weighted graph $G = (\mathcal{V}, \mathcal{E})$, where \mathcal{V} denotes the set of sensor nodes, and \mathcal{E} denotes the set of weighted edges with weight e_{ij} representing the degree of dependency between sensor i and sensor j , which is time-varying. The learned adjacency matrix $\mathbf{A} \in \{0, 1\}^{N \times N}$ captures the structure of this graph, which does not change over time.

Given a multivariate time series segment $\mathbf{X}^t \in \mathbb{R}^{N \times w}$, with w being the size of the window (spanning time steps $t-w$ to $t-1$) used to segment the data, the anomaly detection models described in the previous section decide whether the reading of each sensor at time t is an anomaly. To this end, they simply learn a function $f_\theta(\mathbf{X}^t; \mathbf{A})$ to predict the reading of each sensor at t , given the learned adjacency matrix \mathbf{A} . The training data contains only normal time-series segments, and the model is trained using cross-entropy loss to classify each node as normal or anomalous.

At test time, the anomaly detection model receives a multivariate time series segment and decides whether the data emitted by each sensor in the next time step contains an anomaly by comparing the normalized prediction error against a threshold λ . As a result of this comparison, a vector $\{0, 1\}^N$ is formed, where each element of this vector indicates whether the reading of the respective sensor at t is an anomaly. Since the test data contains real anomalies, BETA aims to degrade the performance of the anomaly detection model by manipulating the anomaly score for the target node $u \in \mathcal{V}$.

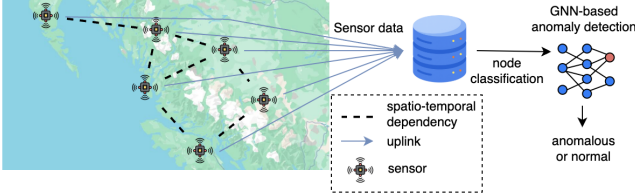


Figure 3: Illustration of a scenario where spatially distributed sensors collect time-series data and transmit it to a GNN-based anomaly detection model deployed on a central node. An attacker may compromise a small number of strategically chosen influencer nodes to add perturbations, misleading the model.

Assumptions. We assume that (1) the GNN-based anomaly detection model is deployed on a central/sink node, receiving data from all sensors in the sensor network, including the target sensor, as depicted in Figure 3; (2) the target sensor is safeguarded and cannot be compromised, unlike the other nodes that can be compromised by the attacker; (3) sensor nodes transmit their data in segments, i.e., they buffer their readings locally and once a full segment is ready, it is sent out; (4) these data transmissions occur asynchronously.

5 THREAT MODEL

To degrade the performance of the deployed GNN-based anomaly detection model, i.e., the *victim model*, the attacker can perturb its input by compromising a subset of the sensors, referred to as *influencer nodes*, which are distinct from the target sensor. The cardinality of the set of influencer nodes is determined based on the attacker's budget. The attacker is capable of intercepting the communication between each sensor node and the sink node. Since segments are transmitted asynchronously by the sensors, the attacker slightly delays the segment transmission by the influencer nodes to create an opportunity to intercept the segments transmitted by the other nodes before transmitting the influencer nodes' segments. This allows the attacker to obtain the full feature matrix \mathbf{X}^t and use it to compute the amount of perturbation that should be added (as described in Algorithm 1).

The attacker operates under a grey-box assumption, with full access to the learned graph structure \mathbf{A} . It also has query access to the victim model f_θ , enabling it to train a *surrogate model* denoted as f_ζ to approximate the victim model's behavior. Yet, it does not have access to the parameters of the victim model, i.e. θ , and does not know its architecture, i.e. the type and number of layers, and activation functions. Moreover, the attacker cannot poison the training data, nor can it change the learned graph structure, e.g. by adding or removing edges. Hence, the attack that we consider in this work is a feature-based, indirect evasion attack against GNNs with known graph structure.

To perform the evasion attack, the attacker generates an adversarial feature matrix $\mathbf{X}'^t = \mathbf{X}^t + \Delta$ by adding a perturbation matrix, Δ , that satisfies three conditions: (1) $\sum_{i=1}^N \mathbb{I}(\|\Delta_i\|_1 \neq 0) \leq B$, with B being the attacker's budget and Δ_i representing the i th row of matrix Δ ; (2) $\|\text{vec}(\Delta)\|_\infty \leq \epsilon$, with $\text{vec}(\cdot)$ being the vectorization operator, to ensure the attack remains imperceptible; and (3) $\Delta_u = 0$, where u is the target sensor. The attacker's goal is to manipulate this

output so that the anomaly detection outcome changes. Formally, this can be written as follows:

$$\mathbb{I}[f_\theta(\mathbf{X}'^t; \mathbf{A})_u > \lambda] \neq \mathbb{I}[f_\theta(\mathbf{X}^t; \mathbf{A})_u > \lambda],$$

where $f_\theta(\mathbf{X}^t; \mathbf{A})_u$ denotes the normalized anomaly score for the target node u . In BETA, a surrogate model guides the selection of the influencer nodes and the computation of Δ .

6 METHODOLOGY

This section introduces BETA, the proposed grey-box evasion attack strategy, and outlines the graph explanation module employed for selecting target nodes (Section 6.1) and the topology-based heuristic used to prune the set of candidate influencer nodes (Section 6.2). Figure 4 describes different steps of BETA, from training a surrogate model, to identifying candidate influential nodes and pruning it, to performing the evasion attack by adding carefully crafted noise to features of these nodes.

Since the attacker does not have knowledge of the victim model, it has to train a surrogate model to approximate the anomaly detection outcome of the victim model for the target node. Using query access to the victim model, the attacker constructs a dataset for training the surrogate model consisting of multiple pairs of historical measurement and node label for the target node, i.e., $\{(\mathbf{X}^t, y_u^{(t)})\}_{t=1, \dots, T}$. Hence, the surrogate model integrates a forecasting module with a threshold based anomaly detection module, which outputs a binary anomaly label in $\{0, 1\}$ for the target node ($0 = \text{normal}$, $1 = \text{anomalous}$).

Algorithm 1 presents the steps of BETA. The first step is to choose the influencer nodes given the attacker's budget B , the adjacency matrix \mathbf{A} , and the surrogate model f_ζ . We explain this process in the following subsections. After obtaining the set of influencer nodes, denoted as \mathcal{V} , and compromising these sensors, the attacker uses PGD to iteratively perturb the node features of the compromised sensors. Specifically, we initialize PGD by uniformly sampling an initial feature matrix from an ℓ_∞ -ball around the original input and masking the elements in that matrix that correspond to the non-influencer nodes. This gives \mathbf{X}_0 defined below:

$$\mathbf{X}_0 = \tilde{\mathbf{X}} \odot \mathbf{S}_{\mathcal{V}}, \quad (13)$$

$$\tilde{\mathbf{X}} \sim \mathcal{B}_\infty(\mathbf{X}^t, \epsilon), \quad \mathcal{B}_\infty(\mathbf{X}^t, \epsilon) = \{\mathbf{X} : \|\text{vec}(\mathbf{X} - \mathbf{X}^t)\|_\infty \leq \epsilon\}, \quad (14)$$

where \odot denotes Hadamard product, and $\mathbf{S}_{\mathcal{V}}$ denotes a binary selector matrix with rows corresponding to the selected influencer nodes are vectors of 1 and other rows are vectors of 0.

At each iteration k , the features are updated in the direction of the gradient of the loss function L , which is the cross-entropy loss between the prediction of the surrogate model f_ζ for the target node u and the true anomaly label of the target node, which is denoted as $\nabla_{\mathbf{X}} L(f_\zeta(\mathbf{X}_k, \mathbf{A})_u, y)$ where \mathbf{X}_k denotes the feature matrix at iteration k , and $\nabla_{\mathbf{X}} L(\cdot)$ computes the gradient of the loss with respect to the input. Finally, the influencer nodes' features are updated according to the PGD update rule:

$$\mathbf{X}_{k+1} = \Pi(\mathbf{X}_k + \alpha \cdot \text{sign}(\nabla_{\mathbf{X}} L(f_\zeta(\mathbf{X}_k, \mathbf{A})_u, y))) \odot \mathbf{S}_{\mathcal{V}}, \quad (15)$$

where α is the step size, $\text{sign}(\cdot)$ denotes the element-wise sign function, and $\Pi(\cdot)$ is the projection operator that ensures the perturbed features remain within the ℓ_∞ -ball around the original input. This iterative update continues until the maximum number of iterations

is reached. Then, the final adversarial feature matrix X'^t is returned. The goal of this update is to maximize the classification loss, i.e., make the model misclassify the target node, while ensuring the perturbations remain small and stealthy.

6.1 Identifying Candidate Influential Nodes

To identify influential nodes for adversarial perturbation, we apply *GAFExplainer* [45] to the surrogate model f_ζ . The surrogate model produces the prediction $y_{O,u}$ for the target node u , together with intermediate node embeddings from each of its L layers. These embeddings are used by GAFExplainer to trace the regions of the graph that most influence the target node's output. GAFExplainer first uses a *node attribute augmentation* module, which uses an attention mechanism to aggregate embeddings from the neighbors of each node, producing enhanced node features that reflect both temporal and structural context. These augmented features are combined with layer-wise GNN embeddings using a *fusion embedding* module. Edge embeddings are then passed through a learnable *weight generator*, followed by a *mask fuser*, which uses a binary concrete distribution to construct a pseudo-discrete mask over the edges. The resulting mask extracts a candidate subgraph, which is re-evaluated by the surrogate GNN to produce a subgraph prediction $y_{S,u}$. The explanation network is trained by minimizing the difference between $y_{S,u}$ and $y_{O,u}$, allowing us to identify the most influential nodes for classifying the target node. This step produces a set of nodes that may exceed the allowable perturbation budget. We introduce a hyperparameter E to control the number of edges that can be kept in the explanation subgraph. Once these top-ranked edges are selected, their incident nodes are automatically included in the subgraph and are treated as the candidate influential nodes. In practice, we choose $E \leq B - 1$, since in the worst case the subgraph is a tree with $E + 1$ nodes which cannot be greater than our attack budget B . As choosing a certain value of E (e.g. $B - 1$) does not guarantee that exactly B nodes will be included in the subgraph, the following step is required to enforce the budget B .

6.2 Pruning Influential Nodes via a Centrality Measure

Once the set of candidate influencer nodes, denoted as \mathcal{V}_S , is produced by GAFExplainer, we further prune it by choosing the top- B influential nodes according to a widely used centrality measure, namely eigenvector centrality [7]. This ensures that the nodes selected for perturbation are not only locally important to the prediction task but also structurally central in the graph. We combine GAFExplainer with eigenvector centrality to ensure the selected nodes are not only relevant to the prediction task but also restricted by the budget, as GAFExplainer may return a subgraph larger than the available budget. This strategy allows the PGD attack to focus on perturbing the most influential nodes as per the budget, thereby improving attack efficiency while maintaining stealthiness by avoiding excessive changes to irrelevant nodes.

Eigenvector centrality assesses a node's importance by considering the centrality of its neighbors. In other words, a node is considered influential if it is connected to other influential nodes. Let vector c collect the eigenvector centrality of all nodes in graph

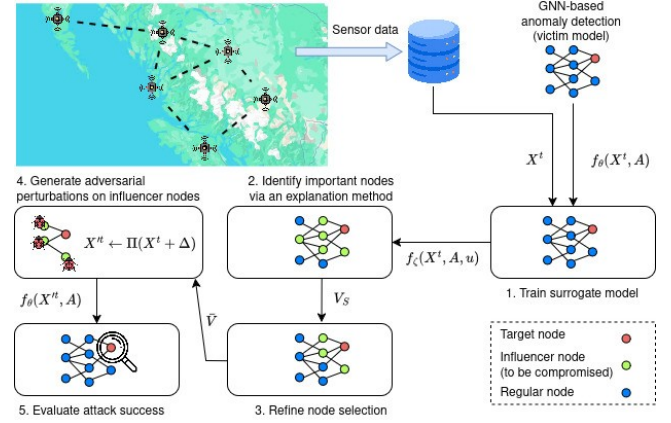


Figure 4: BETA attack pipeline

G. We have $Ac = \lambda_{max}c$ where λ_{max} is the largest eigenvalue of A . We rank the nodes in \mathcal{V}_S according to their eigenvector centrality and select the top B nodes among them. This yields the set of influential nodes, denoted as $\bar{\mathcal{V}}$. The features of these nodes are then perturbed by BETA.

Algorithm 1 BETA: Guided and Constrained PGD Attack

```

1: Input: Adjacency matrix  $A \in \mathbb{R}^{N \times N}$ , Original feature matrix  $X^t \in \mathbb{R}^{N \times w}$ , Surrogate model  $f_\zeta$ , Target node  $u$ , True anomaly label  $y$ , Number of iterations  $K$ , PGD step size  $\alpha$ .
2: Output: Perturbed feature matrix  $X'^t$ 
3:  $\mathcal{V}_S \leftarrow \text{GAFExplainer}(X^t, A, u, E)$   $\triangleright$  Select nodes connected by the top  $E$  important edges
4:  $\bar{\mathcal{V}} \leftarrow \text{SelectTopNodes}(\mathcal{V}_S, B)$   $\triangleright$  Using centrality measures
5: Initialize  $X_0 = \tilde{X} \odot S_{\bar{\mathcal{V}}}$  where  $\tilde{X} \sim \mathcal{B}_\infty(X^t, \epsilon)$ 
6: while  $k < K$  do
7:    $X_{k+1} = \Pi(X_k + \alpha \cdot \text{sign}(\nabla_X L(f_\zeta(X_k, A), y))) \odot S_{\bar{\mathcal{V}}}$ 
8: end while
9: return  $X'^t \leftarrow X_K$ 

```

7 PERFORMANCE EVALUATION

7.1 Datasets

Three publicly available datasets were used in our experiments. Table 2 presents their statistics, including the number of sensor nodes, data points, and the percentage of anomalies.

SWaT (Secure Water Treatment) [29] is a dataset collected from a testbed designed to replicate a six-stage water treatment process in Singapore. It serves as a representative cyber-physical system, integrating 25 sensors, 26 actuators, and programmable logic controllers to monitor and manage the production of clean water. The dataset contains 11 days of sensor readings, including 7 days of normal operations and 4 days involving a range of attack scenarios.

WADI (Water Distribution) [3] extends the SWaT setup by incorporating a network of distribution pipelines. It includes 16 days of operational data: 14 days under normal conditions and 2 days with injected physical attacks. These attacks are staged to simulate malicious behaviors in real-world cyber-physical systems.

Table 2: Statistics of the three datasets used in experiments

Dataset	#Nodes	#Train	#Test	Anomalies
SJVAir	41	98,381	35,663	25%
SWaT	51	47,515	44,986	11.97%
WADI	127	118,795	17,275	5.99%

SJVAir [1] contains PM2.5 concentration measurements ($\mu\text{g}/\text{m}^3$) collected at two-minute intervals from air quality sensors deployed across the city of Fresno in California. The collected data is pre-processed by aggregating the two-minute readings into hourly averages. Sensors with more than one hour of consecutive missing data were excluded, resulting in a total of 41 sensors, each contributing 2,928 hourly measurements. Additionally, historical wind data [2] for Fresno, comprising hourly wind speed and direction, is obtained from Visual Crossing for the same time period. This meteorological data is aligned with the sampling frequency of the PM2.5 dataset to support multimodal analysis. To evaluate model robustness, we injected synthetically generated anomalies into the test data to simulate short bursts of random noise in sensor readings. These perturbations are sampled from a zero-mean Gaussian distribution, $\mathcal{N}(0, \zeta^2 I_{L \times L})$, where $\zeta = 10$ determines the intensity of the noise, and L is the anomaly duration drawn from the Poisson distribution with mean $\lambda_{\text{var}} = 7$. The identity matrix $I_{L \times L}$ ensures that the noise is uncorrelated across the L time steps.

7.2 Evaluation Metrics

We study an adversarial setting using two GNN-based victim models, GDN [14] and TopoGDN [25], which serve as strong baselines for multivariate time series anomaly detection. We assess anomaly detection performance using F1 Score and Area Under the Precision-Recall Curve (AUC-PR) as metrics. Additionally, we use the Fractional Target Accuracy (FTA) metric which was used in prior work [48]. We define these metrics below:

F1 Score. Given the class imbalance typical in anomaly detection tasks, we compute the F1 Score to effectively balance precision and recall. The F1 Score is defined as:

$$F1 = \frac{2 \cdot \text{Precision} \cdot \text{Recall}}{\text{Precision} + \text{Recall}}$$

where

$$\text{Precision} = \frac{TP}{TP + FP}, \quad \text{Recall} = \frac{TP}{TP + FN}$$

Here, TP , FP , and FN represent the number of true positives, false positives, and false negatives, respectively.

AUC-PR [24]. In highly imbalanced tasks like anomaly detection, evaluating the trade-off between precision and recall is critical, where the trade-off is normally obtained by adjusting the decision threshold (λ). In our case, the threshold is chosen from the maximum validation error on normal data and therefore varies across datasets. Unlike AUC-ROC, which accounts for true negatives, AUC-PR focuses solely on the positive class, making it more appropriate when anomalies are rare. A higher AUC-PR indicates that the model maintains high precision while achieving strong recall, reflecting effective detection performance in sparse anomaly settings.

FTA. To evaluate the robustness of the anomaly detection model under adversarial attack, we define the FTA metric which measures the proportion of target nodes whose anomaly classification remains correct after perturbation, relative to the ground truth. For each target node, predictions are made at each time step using a sliding window of size w , and the node is considered correctly classified if its binary anomaly decision (based on a predefined threshold λ) matches the ground-truth label across the evaluated time steps. Note that FTA decreases as the attack success rate increases.

In our implementation, the anomaly detection threshold (λ) is defined as the maximum error score observed on the validation set. These thresholds are specifically used for computing F1 score and FTA metrics. For the GDN model, the thresholds are 22.22 for SJVAir, 26.42 for SWaT and 26.67 for WADI. In comparison, for the TopoGDN model, the thresholds are 15.19 for SJVAir, 20.90 for SWaT and 19.33 for WADI. To evaluate the attack success rate, PGD is performed with a step size of $\alpha = 0.01$ for $t = 10$ iterations, to generate adversarial perturbations for assessing the model's robustness.

7.3 Baselines

7.3.1 Random attack. In the random attack, the target node is the same as in the other attack strategies. Only B influencer nodes are randomly selected from the graph (excluding the target) and their features are randomly perturbed. To perturb these influencer nodes, uniform noise is added to their features. Specifically, each selected feature is replaced with a new value drawn from a uniform distribution $\mathcal{U}(\min_j, \max_j)$, where \min_j and \max_j denote the minimum and maximum values of feature j across the dataset.

7.3.2 Nettack [48]. The original graph $G = (V, \mathcal{E})$ is transformed into an adversarial version $G' = (V, \mathcal{E}')$ with a modified feature matrix X'^t , such that a designated *target node* u is misclassified by the GNN model. The attack introduces minimal yet effective perturbations by modifying a small subset of *attacker nodes*. The attacker nodes are chosen based on how much each neighbour of the target node u influences its classification. To do this, Nettack approximates the effect of modifying each candidate edge by computing the output logits using the second-order adjacency matrix and the node feature weights. For each candidate edge, it then calculates a score as the difference between the logits of the true class of the target node and the maximum logit of all incorrect classes. To ensure the true class does not affect the max operation, its logit is suppressed by subtracting a large constant. Edges that receive lower scores are those that reduce the model's confidence in the correct label, making them stronger candidates for attack. By ranking the neighbours with this score, Nettack selects the top- B influencer nodes to manipulate during the attack.

Nettack consists of two types of modifications: (1) Feature Manipulation, which alters the node feature matrix X^t to deceive the model's decision process, and (2) Structural Modification, which updates the edge set \mathcal{E} by adding or removing edges, thereby affecting the neighborhood context and information propagation around the target node. These changes are crafted to maintain stealth under a constrained perturbation budget while successfully altering the model's prediction. For a fair comparison with BETA which is a feature-based evasion attack, we implement a variant of Nettack

Table 3: Anomaly detection performance in terms of F1 Score, AUC-PR and FTA for the GDN model under different adversarial attack strategies on SJVAir, SWaT, and WADI datasets.

Method	SJVAir			SWaT			WADI		
	F1	AUC-PR	FTA	F1	AUC-PR	FTA	F1	AUC-PR	FTA
No attack	0.9794	0.8250	0.8566	0.8521	0.9136	0.8364	0.7896	0.7848	0.9015
Random	0.3654	0.7243	0.7490	0.5737	0.8744	0.7261	0.5413	0.6998	0.8815
Nettack	0.3526	0.6787	0.6557	0.5442	0.8338	0.6111	0.5303	0.5833	0.7989
<i>Ablation:</i> PGD + Heuristics	0.3461	0.5797	0.6141	0.4108	0.7176	0.5517	0.5234	0.4704	0.7543
<i>Ablation:</i> Nettack + GAFExplainer	0.2899	0.5497	0.3854	0.4034	0.5560	0.4425	0.5134	0.4667	0.7279
BETA (Ours)	0.2786	0.4392	0.3032	0.3757	0.5060	0.4330	0.4531	0.4110	0.6836

Table 4: Anomaly detection performance in terms of F1 Score, AUC-PR and FTA for the TopoGDN model under different adversarial attack strategies on SJVAir, SWaT, and WADI datasets.

Method	SJVAir			SWaT			WADI		
	F1	AUC-PR	FTA	F1	AUC-PR	FTA	F1	AUC-PR	FTA
No attack	0.8480	0.9204	0.8752	0.8774	0.8903	0.8931	0.9048	0.9192	0.9854
Random	0.7880	0.7428	0.7881	0.8028	0.8840	0.7993	0.8025	0.8342	0.9650
Nettack	0.7219	0.7033	0.6852	0.7206	0.8463	0.7835	0.7727	0.8138	0.9362
<i>Ablation:</i> PGD + Heuristics	0.6353	0.5903	0.6564	0.6764	0.8300	0.7203	0.7211	0.7806	0.9136
<i>Ablation:</i> Nettack + GAFExplainer	0.5829	0.5576	0.5802	0.5659	0.7147	0.6533	0.6154	0.6365	0.7963
BETA (Ours)	0.5532	0.4566	0.4547	0.4390	0.5893	0.6418	0.5557	0.6153	0.7387

that performs feature manipulation only, without altering the graph structure.

Nettack + GAFExplainer. In this variant, we use GAFExplainer (Section 6.1) to identify the top-B most influential nodes with respect to the target node, based on their contribution to the GNN’s prediction. These candidate nodes are then refined using a centrality based selection strategy (Section 6.2) and the resulting set is chosen as the final influencer nodes. Nettack’s feature perturbation strategy is applied to these influencer nodes to mislead the model’s prediction for the target node. Unlike the original Nettack, which uses a heuristic scoring mechanism to select attacker nodes, this variant integrates our proposed explainability-guided node selection strategy. Thus, this baseline is used as an ablation to see how effective constrained PGD is compared with Nettack’s way of changing features.

PGD + Heuristics. This variant combines our constrained PGD attack with the influencer node selection strategy from Nettack. Once these nodes are selected, PGD attack is applied to their features to craft adversarial examples that stay within a perturbation budget and preserve stealth, while maximizing the chance of misclassifying the target node. Thus, this baseline is used as an ablation to see how effective our node selection is compared to the heuristics used in Nettack.

BETA (Unbudgeted). In this variant, we apply BETA in a non-budgeted setting, allowing unrestricted use of influencer nodes during the attack. Specifically, we assume all nodes in the graph, except the target node, are influencer nodes. This setup helps assess the upper-bound performance of our attack when not constrained by a budget.

7.4 Experimental Setup

We implement GDN and TopoGDN using PyTorch [32], following the authors’ implementation of GDN¹ and TopoGDN². The Nettack implementation is adapted from its public repository to remove the structural modification component, which is not applicable for feature-based attacks³. For GAFExplainer, we use the public repository provided by the authors⁴. We follow the preprocessing strategy adopted in TopoGDN [25], applying Min-Max normalization to scale all sensor readings to the [0,1] range. In PGD attacks, we perform independent trials, each initialized from a random point within the ℓ_∞ -ball around the original input. Specifically, we start from 5 randomly selected feature matrices, i.e. \tilde{X} . We assume that perturbations that have an ℓ_∞ norm smaller than $\epsilon = 0.1$ are imperceptible. We segment the time series using a sliding window of size 100 with a stride of 10. The model is trained using the Adam optimizer with a learning rate of 0.001 and a batch size of 32. All models are trained on an NVIDIA RTX 2080 TI GPU.

8 RESULTS AND ANALYSIS

We evaluate the performance of several attack strategies, including random attack, Nettack, BETA, and its variants, across 3 datasets using F1 Score, AUC-PR and FTA.

¹<https://github.com/d-ailin/GDN>

²<https://github.com/ljj-cyber/TopoGDN/tree/main>

³<https://github.com/danielzuegner/nettack>

⁴<https://github.com/wyhi/GAFExplainer>

8.1 Attack Success Evaluation

Table 3 reports the anomaly detection performance of GDN under different adversarial attacks with $B = 5$, in the SJVAir, SWaT, and WADI datasets using F1 Score, AUC-PR and FTA. When sensor data are not perturbed (i.e. no attack), GDN exhibits strong anomaly detection performance, with high F1, AUC-PR, and FTA scores in all datasets. Random attack leads to the smallest drop in anomaly detection performance, especially in terms of AUC-PR and FTA, compared to other attacks. On the SJVAir dataset, BETA reduces the F1 score to 0.2786, AUC-PR to 0.4392, and FTA to 0.3032, compared to 0.3526, 0.6787, and 0.6557 under Nettack, a substantial drop in all performance metrics. Similarly, on the SWaT dataset, BETA lowers the F1 score from 0.5442 (Nettack) to 0.3757, AUC-PR from 0.8338 to 0.5060 and FTA from 0.6111 to 0.4330, highlighting its ability to mislead the model more effectively than Nettack or its variants. On the WADI dataset, although the drop is less significant, BETA still achieves the lowest F1 (0.4531) and AUC-PR (0.4110) among all methods, while reducing FTA to 0.6836 from 0.7989.

The comparison with PGD + Heuristics and Nettack + GAFExplainer reveals the efficacy of each individual component of BETA, namely PGD as the attack strategy and GAFExplainer as the influencer node selection method. PGD + Heuristics improves over Nettack by applying gradient-based perturbations to node features. Nettack + GAFExplainer uses the explanation technique to guide node selection, yielding stronger attack performance than Random, Nettack and even PGD + Heuristics. This suggests that the improvement in attack success rate is largely due to the way that the influencer nodes are selected. Overall, BETA demonstrates superior capability in concealing true anomalies and consistently compromising the robustness of the GDN model, achieving up to 21.53% higher FTA compared to Nettack.

Table 4 presents the performance degradation of TopoGDN under different adversarial attacks for $B = 5$. In the absence of any adversarial attacks, TopoGDN consistently achieves high performance, with F1, AUC-PR and FTA scores exceeding 80%. For the attack scenarios, BETA shows the strongest performance and the ranking of the baseline methods remains the same as the one for GDN. While TopoGDN exhibits higher robustness to adversarial attacks than GDN, BETA can still cause a significant drop in its anomaly detection performance.

8.2 Sensitivity to the Attack Budget

We compare the effectiveness of various attack strategies under varying perturbation budgets using the FTA metric. We first focus on the effectiveness of the attack strategies against the GDN model as the number of influencer nodes increases from 1 to 6. As shown in Figure 5, a clear trend emerges across all three datasets: larger attack budgets lead to lower FTA scores, indicating stronger adversarial impact. In this setting, the Random attack exerts the weakest effect on FTA, while Nettack + GAFExplainer generally yields the lowest FTA among the baselines, making it the strongest baseline attack strategy. BETA consistently achieves the lowest FTA across all budgets, underscoring the advantage of combining graph explanations with PGD-based optimization. A closer inspection of the results across individual datasets reveals distinct patterns.

In SJVAir, the high anomaly density makes simple attacks effective, causing Nettack and PGD + Heuristics to yield comparable results. In case of SWaT, with $B = 3, 4, 5$, PGD + Heuristics and Nettack + GAFExplainer perform very similar since one benefits from stronger feature perturbations and the other from better node selection. The SWaT dataset exhibits stronger robustness to adversarial attacks than SJVAir, with higher overall FTA under attack, although BETA still achieves significant degradation in the performance of GDN at larger budgets. WADI, on the other hand, demonstrates the strongest robustness to adversarial attacks, as reflected by higher FTA values and narrower performance gaps between attack strategies.

Next, we examine the performance gap between BETA and the strongest baseline, i.e. Nettack + GAFExplainer, and the unbudgeted variant of BETA across different datasets. In SJVAir, BETA decreases FTA from 0.4978 at $B = 1$ to 0.2544 at $B = 6$, while Nettack + GAFExplainer drops from 0.5792 to 0.3403. In SJVAir, the FTA under BETA at $B = 6$ is close to the unbudgeted case (0.2298), suggesting that even a small number of strategically chosen influencer nodes would suffice to launch a powerful attack. In SWaT, BETA reduces FTA from 0.6801 at $B = 1$ to 0.3755 at $B = 6$, compared to Nettack + GAFExplainer, where FTA declines from 0.7126 to 0.5084. The FTA under the unbudgeted variant of BETA is 0.2816. In WADI, the largest dataset with the lowest anomaly ratio, the FTA under BETA falls from 0.8775 at $B = 1$ to 0.6181 at $B = 6$, while the FTA under Nettack + GAFExplainer decreases from 0.9145 to 0.6439. Here, the gap between FTA values is relatively small. Nevertheless, BETA consistently outperforms across all budgets.

Figure 6 compares the performance of these attack strategies against the TopoGDN model, with varying budgets ($B = 1-6$). It can be readily seen that TopoGDN is slightly more robust to feature-based evasion attacks than GDN, and as with GDN, larger budgets lead to lower FTA. Among the baselines, the Random attack remains the weakest, Nettack and PGD + Heuristics cause moderate degradation, and Nettack + GAFExplainer consistently performs best. BETA once again beats all baselines in terms of FTA, establishing itself as the strongest attack across all datasets. In SJVAir, BETA reaches FTA of 0.3848 with 6 influencer nodes, compared to 0.4815 reached by Nettack + GAFExplainer (almost 10% gap), with the unbudgeted case lowering FTA further to 0.2963. In SWaT, TopoGDN maintains higher FTA overall, but BETA still achieves significant degradation at $B = 6$ (FTA=0.5900), although there is a wider gap between BETA and its unbudgeted variant (FTA=0.2874). In WADI, the Random attack barely affects FTA (0.9979 → 0.9630). Nevertheless, BETA reduces FTA to 0.6605 at $B = 6$, compared to FTA of 0.7840 achieved by Nettack + GAFExplainer. The gap between BETA and its unbudgeted variant is quite large in this case, implying that more influencer nodes would be needed to fully confuse the model in this specific case.

8.3 Evaluating Centrality Measures for Pruning Influencer Nodes

Table 5 presents the impact of various centrality-based node selection strategies that can be used for pruning the set of influencer nodes obtained from GAFExplainer on the effectiveness of BETA for different numbers of influencer nodes ($B = 3$ to $B = 6$) on

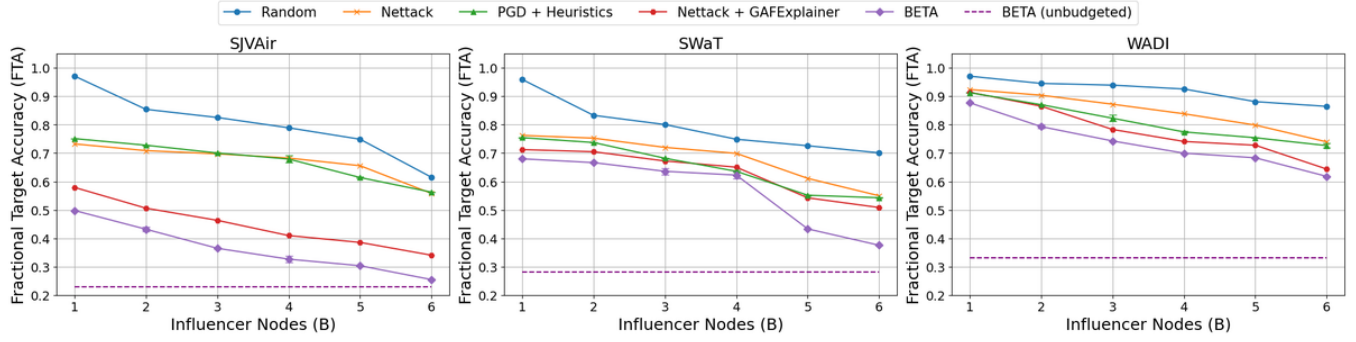


Figure 5: FTA comparison of attack methods with varying influencer nodes on the GDN model using SJVAir, SWaT and WADI dataset. Error bars show standard deviation across 5 runs.

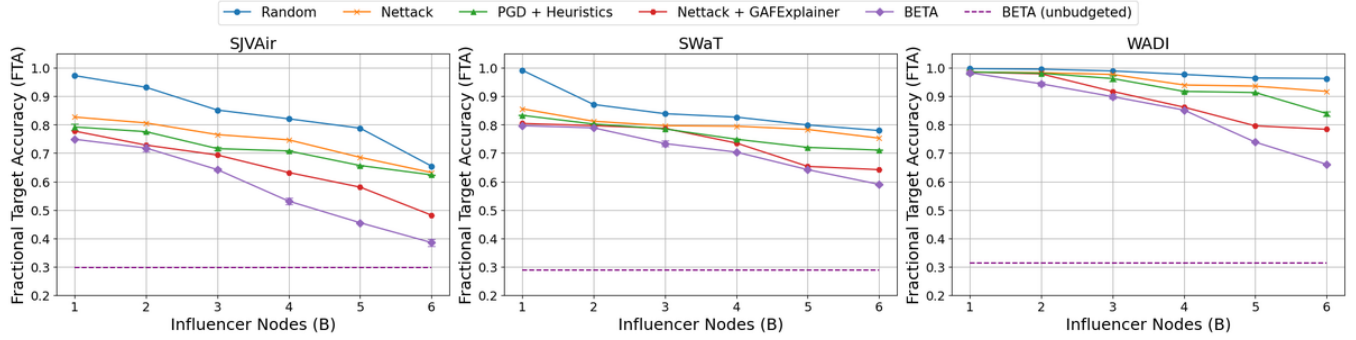


Figure 6: FTA comparison of attack methods with varying influencer nodes on the TopoGDN model using SJVAir, SWaT and WADI dataset. Error bars show standard deviation across 5 runs.

the SJVAir dataset. In particular, we rank nodes in \mathcal{V}_S using centrality measures such as node degree, closeness centrality [4, 5], eigenvector centrality [6, 7], betweenness centrality [43], clustering coefficient [8, 23] and average neighbour degree of node. For all budgets, we find that selecting influencer nodes based on *eigenvector centrality* consistently results in the lowest FTA, highlighting its superior ability to identify influential nodes for maximizing attack effectiveness. For instance, at $B = 6$, eigenvector-based selection achieves an FTA of 0.2011, outperforming all others. This trend remains consistent across other values of B . This result confirms that eigenvector centrality is more effective in capturing nodes that exert higher indirect influence over the target node's prediction, thereby enhancing the impact of the constrained PGD attack guided by GAFExplainer.

8.4 Impact of GAFExplainer-Based Guidance on Centrality-Based Node Selection

We investigate if combining GAFExplainer and eigenvector centrality results in a better influencer node selection scheme than using eigenvector centrality alone. To this end, we fix the attack budget, B , and evaluate the performance of GDN in terms of FTA on the SJVAir dataset, using two node selection schemes in BETA. As shown in Figure 7, using only eigenvector centrality yields higher FTA values, ranging from 0.4464 for $B = 3$ to 0.3725 for $B = 6$, indicating weaker attacks. In contrast, combining GAFExplainer with centrality consistently lowers FTA, starting from 0.3029 for

Table 5: Impact of centrality metrics on attack effectiveness across different influencer node configurations on the GDN model for the SJVAir dataset.

Centrality measure	$B = 3$	$B = 4$	$B = 5$	$B = 6$
Eigenvector	0.3029	0.3011	0.2630	0.2011
Degree	0.3962	0.3043	0.2836	0.2398
Clustering Coefficient	0.3998	0.3410	0.3005	0.2167
Betweenness	0.3634	0.3235	0.3013	0.2521
Closeness	0.3469	0.3125	0.2761	0.2504
Avg. Neighbor Degree	0.3635	0.3675	0.2701	0.2048

$B = 3$ to 0.2011 for $B = 6$, indicating stronger attacks. The result confirms that choosing a subgraph using GAFExplainer and pruning it according to eigenvector centrality is better than directly selecting influencer nodes using eigenvector centrality.

9 CONCLUSION

This paper introduces BETA, a novel budgeted evasion attack that perturbs only node features in multivariate time series graphs to mislead GNN-based anomaly detectors, either by triggering false alarms or concealing true anomalies. Without altering the graph structure, BETA succeeds in performing effective indirect attacks by adding small perturbations to sensor readings from a carefully

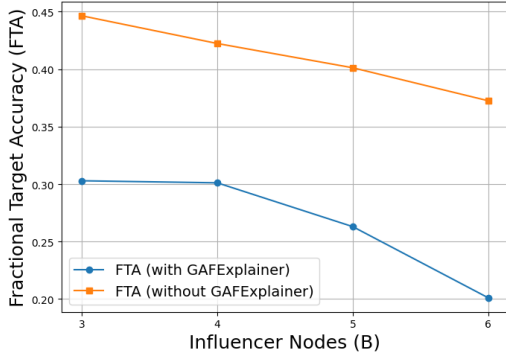


Figure 7: Impact of combining GAFExplainer and Eigenvector Centrality for selecting the influencer nodes on the GDN model for the SJVAir dataset

chosen set of influencer nodes, exposing the vulnerability of GNN models even when the target node itself is safeguarded. Future work will focus on developing robust defenses against such attacks, including graph smoothing, adversarial training, and explainability-guided strategies.

REFERENCES

- [1] 2024. SJVAir. Official Website. <https://www.sjvair.com/>. Accessed: 2024-07-21.
- [2] 2024. Visual Crossing. Historical Weather Data & Weather Forecast Data. <https://www.visualcrossing.com/weather-data>.
- [3] Chuadhy Mujeeb Ahmed, Venkata Reddy Palleli, and Aditya P. Mathur. 2017. WADI: a water distribution testbed for research in the design of secure cyber physical systems. In *Proceedings of the 3rd International Workshop on Cyber-Physical Systems for Smart Water Networks* (Pittsburgh, Pennsylvania) (*CySWATER '17*). Association for Computing Machinery, New York, NY, USA, 25–28. <https://doi.org/10.1145/3055366.3055375>
- [4] Alex Bavelas. 1950. Communication patterns in task-oriented groups. *Journal of the acoustical society of America* (1950).
- [5] Murray A Beauchamp. 1965. An improved index of centrality. *Behavioral science* 10, 2 (1965), 161–163.
- [6] Phillip Bonacich. 1972. Factoring and weighting approaches to status scores and clique identification. *Journal of mathematical sociology* 2, 1 (1972), 113–120.
- [7] Phillip Bonacich. 2007. Some unique properties of eigenvector centrality. *Social networks* 29, 4 (2007), 555–564.
- [8] Stephen P Borgatti and Martin G Everett. 1997. Network analysis of 2-mode data. *Social networks* 19, 3 (1997), 243–269.
- [9] Yulong Cao, Chaowei Xiao, Benjamin Cyr, Yimeng Zhou, Won Park, Sara Rampazzi, Qi Alfred Chen, Kevin Fu, and Z Morley Mao. 2019. Adversarial sensor attack on lidar-based perception in autonomous driving. In *Proceedings of the 2019 ACM SIGSAC conference on computer and communications security*. 2267–2281.
- [10] Nicholas Carlini and David Wagner. 2017. Towards evaluating the robustness of neural networks. In *2017 ieee symposium on security and privacy (sp)*. Ieee, 39–57.
- [11] Liang Chen, Jintang Li, Jiaying Peng, Tao Xie, Zengxu Cao, Kun Xu, Xiangnan He, Zibin Zheng, and Bingzhe Wu. 2020. A survey of adversarial learning on graphs. *arXiv preprint arXiv:2003.05730* (2020).
- [12] Zekai Chen, Dingshuo Chen, Xiao Zhang, Zixuan Yuan, and Xiuzhen Cheng. 2021. Learning graph structures with transformer for multivariate time-series anomaly detection in IoT. *IEEE Internet of Things Journal* 9, 12 (2021), 9179–9189.
- [13] Hanjun Dai, Hui Li, Tian Tian, Xin Huang, Lin Wang, Jun Zhu, and Le Song. 2018. Adversarial attack on graph structured data. In *International conference on machine learning*. PMLR, 1115–1124.
- [14] Ailin Deng and Bryan Hooi. 2021. Graph neural network-based anomaly detection in multivariate time series. In *Proceedings of the AAAI conference on artificial intelligence*, Vol. 35. 4027–4035.
- [15] Ian J Goodfellow, Jonathon Shlens, and Christian Szegedy. 2014. Explaining and harnessing adversarial examples. *arXiv preprint arXiv:1412.6572* (2014).
- [16] Adam Goodge, Bryan Hooi, See Kiong Ng, and Wee Siong Ng. 2021. Robustness of autoencoders for anomaly detection under adversarial impact. In *Proceedings of the twenty-ninth international conference on international joint conferences on artificial intelligence*. 1244–1250.
- [17] Thi Kieu Khanh Ho, Ali Karami, and Narges Armanfard. 2025. Graph Anomaly Detection in Time Series: A Survey. *IEEE Transactions on Pattern Analysis and Machine Intelligence* 47, 8 (2025), 6990–7009.
- [18] Yifan Jia, Jingyi Wang, Christopher M Poskitt, Sudipta Chattopadhyay, Jun Sun, and Yuqi Chen. 2021. Adversarial attacks and mitigation for anomaly detectors of cyber-physical systems. *International Journal of Critical Infrastructure Protection* 34 (2021), 100452.
- [19] Ming Jin, Huan Yee Koh, Qingsong Wen, Daniele Zambon, Cesare Alippi, Geoffrey I Webb, Irwin King, and Shirui Pan. 2024. A survey on graph neural networks for time series: Forecasting, classification, imputation, and anomaly detection. *IEEE Transactions on Pattern Analysis and Machine Intelligence* (2024).
- [20] Hwan Kim, Byung Suk Lee, Won-Yong Shin, and Sungsu Lim. 2022. Graph anomaly detection with graph neural networks: Current status and challenges. *IEEE Access* 10 (2022), 111820–111829.
- [21] Alexey Kurakin, Ian Goodfellow, and Samy Bengio. 2016. Adversarial machine learning at scale. *arXiv preprint arXiv:1611.01236* (2016).
- [22] Jongsoo Lee, Byeongtae Park, and Dong-Kyu Chae. 2023. Duogat: Dual time-oriented graph attention networks for accurate, efficient and explainable anomaly detection on time-series. In *Proceedings of the 32nd ACM International Conference on Information and Knowledge Management*. 1188–1197.
- [23] Pedro G Lind, Marta C Gonzalez, and Hans J Herrmann. 2005. Cycles and clustering in bipartite networks. *Physical Review E—Statistical, Nonlinear, and Soft Matter Physics* 72, 5 (2005), 056127.
- [24] Qinghua Liu and John Paparrizos. 2024. The elephant in the room: Towards a reliable time-series anomaly detection benchmark. *Advances in Neural Information Processing Systems* 37 (2024), 108231–108261.
- [25] Zhe Liu, Xiang Huang, Jingyun Zhang, Zhifeng Hao, Li Sun, and Hao Peng. 2024. Multivariate time-series anomaly detection based on enhancing graph attention networks with topological analysis. In *Proceedings of the 33rd ACM International Conference on Information and Knowledge Management*. 1555–1564.
- [26] Xiaoxiao Ma, Jia Wu, Shan Xue, Jian Yang, Chuan Zhou, Quan Z Sheng, Hui Xiong, and Leman Akoglu. 2021. A comprehensive survey on graph anomaly detection with deep learning. *IEEE transactions on knowledge and data engineering* 35, 12 (2021), 12012–12038.
- [27] Srinidhi Madabhushi and Rinku Dewri. 2025. Mitigating Over-Generalization in Anomalous Power Consumption Detection using Adversarial Training. *ACM Transactions on Cyber-Physical Systems* (2025).
- [28] Aleksander Madry, Aleksandar Makelov, Ludwig Schmidt, Dimitris Tsipras, and Adrian Vladu. 2017. Towards deep learning models resistant to adversarial attacks. *arXiv preprint arXiv:1706.06083* (2017).
- [29] Aditya P Mathur and Nils Ole Tippenhauer. 2016. SWaT: A water treatment testbed for research and training on ICS security. In *2016 international workshop on cyber-physical systems for smart water networks (CySWater)*. IEEE, 31–36.
- [30] Apostolos Modas, Ricardo Sanchez-Matilla, Pascal Frossard, and Andrea Cavallaro. 2020. Toward robust sensing for autonomous vehicles: An adversarial perspective. *IEEE Signal Processing Magazine* 37, 4 (2020), 14–23.
- [31] John Paparrizos, Yuhan Kang, Paul Boniol, Ruey S. Tsay, Themis Palpanas, and Michael J. Franklin. 2022. TSB-UAD: an end-to-end benchmark suite for univariate time-series anomaly detection. *Proc. VLDB Endow.* 15, 8 (April 2022), 1697–1711.
- [32] A Paszke. 2019. Pytorch: An imperative style, high-performance deep learning library. *arXiv preprint arXiv:1912.01703* (2019).
- [33] Aikaterini Protopero, Stavros Papadopoulos, Anastasios Drosou, Dimitrios Tzovaras, and Ioannis Refanidis. 2021. A graph neural network method for distributed anomaly detection in IoT. *Evolving Systems* 12, 1 (2021), 19–36.
- [34] Abdul Kalam Shaik, Amitansu Das, and Venkata Reddy Palleli. 2025. Study of Adversarial Attacks on Anomaly Detectors In Industrial Control Systems. Available at ssrn.com/abstract=5126158 (2025).
- [35] Jiawei Su, Danilo Vasconcellos Vargas, and Kouichi Sakurai. 2019. One Pixel Attack for Fooling Deep Neural Networks. *IEEE Transactions on Evolutionary Computation* 23, 5 (2019), 828–841.
- [36] Lichao Sun, Yingtong Dou, Carl Yang, Kai Zhang, Ji Wang, S Yu Philip, Lifang He, and Bo Li. 2022. Adversarial attack and defense on graph data: A survey. *IEEE Transactions on Knowledge and Data Engineering* 35, 8 (2022), 7693–7711.
- [37] Shahrooz Tariq, Binh M Le, and Simon S Woo. 2022. Towards an Awareness of Time Series Anomaly Detection Models' Adversarial Vulnerability. In *Proceedings of the 31st ACM International Conference on Information & Knowledge Management*. 3534–3544.
- [38] Shreshth Tuli, Giuliano Casale, and Nicholas R Jennings. 2022. Tranad: Deep transformer networks for anomaly detection in multivariate time series data. *arXiv preprint arXiv:2201.07284* (2022).
- [39] Petar Veličković, Guillem Cucurull, Arantxa Casanova, Adriana Romero, Pietro Lio, and Yoshua Bengio. 2017. Graph attention networks. *arXiv preprint arXiv:1710.10903* (2017).
- [40] Aristidis G Vrahatis, Konstantinos Lazaros, and Sotiris Kotsiantis. 2024. Graph attention networks: a comprehensive review of methods and applications. *Future Internet* 16, 9 (2024), 318.
- [41] Xiang Wang, Xiangnan He, Yixin Cao, Meng Liu, and Tat-Seng Chua. 2019. Kgat: Knowledge graph attention network for recommendation. In *Proceedings of the 25th ACM SIGKDD international conference on knowledge discovery & data mining*. 950–958.

- [42] Xiao Wang, Houye Ji, Chuan Shi, Bai Wang, Yanfang Ye, Peng Cui, and Philip S Yu. 2019. Heterogeneous graph attention network. In *The world wide web conference*. 2022–2032.
- [43] Stanley Wasserman and Katherine Faust. 1994. Social network analysis: Methods and applications. (1994).
- [44] Yulei Wu, Hong-Ning Dai, and Haina Tang. 2021. Graph neural networks for anomaly detection in industrial Internet of Things. *IEEE Internet of Things Journal* 9, 12 (2021), 9214–9231.
- [45] Zhitao Ying, Dylan Bourgeois, Jiaxuan You, Marinka Zitnik, and Jure Leskovec. 2019. Gnnexplainer: Generating explanations for graph neural networks. *Advances in neural information processing systems* 32 (2019).
- [46] He Zhang, Bang Wu, Xiangwen Yang, Chuan Zhou, Shuo Wang, Xingliang Yuan, and Shirui Pan. 2021. Projective ranking: A transferable evasion attack method on graph neural networks. In *Proceedings of the 30th ACM International Conference on Information & Knowledge Management*. 3617–3621.
- [47] Xiaona Zhou, Constantin Brif, and Ismini Lourentzou. 2025. mTSBench: Benchmarking Multivariate Time Series Anomaly Detection and Model Selection at Scale. *arXiv preprint arXiv:2506.21550* (2025).
- [48] Daniel Zügner, Amir Akbarnejad, and Stephan Günnemann. 2018. Adversarial attacks on neural networks for graph data. In *Proceedings of the 24th ACM SIGKDD international conference on knowledge discovery & data mining*. 2847–2856.
- [49] Daniel Zügner and Stephan Günnemann. 2024. Adversarial Attacks on Graph Neural Networks via Meta Learning. *arXiv:1902.08412 [cs.LG]* <https://arxiv.org/abs/1902.08412>